information services
gwasanaethau gwybodaeth

Enhancement in the rate of nitrate degradation on Au- and Ag-decorated TiO$_2$ photocatalysts

Thomas Caswell,[a] Mbongiseni W. Dlamini,[a] Peter J. Miedziak,[a,b] Samuel Pattisson,[a] Philip R. Davies,[a] Stuart H. Taylor,[a] Graham J. Hutchings[a*]

[a]Cardiff Catalysis Institute, School of Chemistry, Cardiff University, Park Place, Cardiff, CF10 3AT, UK

[b]School of Applied Sciences, University of South Wales, Pontypridd CF37 4AT, UK

*Corresponding author: hutch@cardiff.ac.uk (GJ Hutchings)

Abstract

The solar-driven reduction of nitrate to nitrogen has been studied in the presence of a formate hole scavenger, over a series of Au- and Ag-decorated TiO$_2$ catalysts. In this study, the catalyst preparation protocol was found to influence the nitrate transformation in the order: incipient wetness impregnation > stabilizer-free sol immobilization > sol immobilization. However, the sequence of performing specific treatment steps such as drying, calcination and sieving had a less pronounced effect. Low-conversion conditions were utilized to study the photo-degradation of nitrate over a range of monometallic and bimetallic catalysts with metal concentrations in the range M = 0 − 1 wt.% (M: Au, Ag, Pd, AuAg). Our findings demonstrate that selectively degrading nitrate to N$_2$ over these co-catalysts is non-trivial and is metal content dependent. For Au-doped TiO$_2$ catalysts, the highest activity was measured over 0.2 wt.% Au/TiO$_2$ while a higher metal loading of 0.4 wt.% was required for the Ag/TiO$_2$ photocatalyst. Product selectivity was also demonstrated to be dependent on metal and metal loading: approximately 22 % ammonium selectivity was determined over a 0.1 wt.% Ag-doped catalysts, however this product was not detected when utilising Au-doped catalysts. Total selectivity to dinitrogen was shown to be possible on both Au and Ag doped catalysts, and again this was dependent on the concentration of the metal (Ag > 0.3 wt.%; 0.2 < Au ≥ 0.4 wt.%).

Keywords:

photocatalysis; nitrate; water remediation; gold catalysis, silver catalysts

1   Introduction

Anthropogenic activities have significantly altered the nitrogen cycle in the past few decades and, as a result, nitrate concentration in water systems has been increasing. [1, 2] The concern regarding elevated nitrate concentration in drinking water is particularly serious in less developed communities, where runoffs from nitrogen-rich fertilizers, pesticides, poorly treated sewage effluent and concentrated animal feeding operations can accumulate nitrate in surface and groundwater aquifers. Ingestion of nitrate-contaminated waters has been linked with several potentially fatal public health risks, such as infant methemoglobinemia (blue baby syndrome), hypertension, leukaemia, disruption of thyroid function, diabetes and the production of carcinogenic N-nitroso compounds within the gastrointernal tract.[3-6] Nitrate is also responsible for environmental issues such as algal blooms and eutrophication which depletes oxygen in water bodies thus affecting aquatic ecosystems. With these considerations, the United States Environmental Protection Agency and the European Community established maximum contamination levels (MCL) of 10 mg-N/L and 11.3 mg-N/L of nitrate nitrogen in drinking water, respectively.[7]

Efficient removal of nitrates, also called denitrification, from surface and ground waters is still a global challenge. Denitrification approaches commonly utilized are based on reverse osmosis,[8, 9] ion exchange and electrodialysis[10] technologies. While these physicochemical methods continue to be used, they do not entirely solve the problem as they concentrate the nitrate into brines as opposed to degrading it to harmless species such as nitrogen. Other methods such as catalytic reduction, photolysis[11, 12] and biological denitrification have also been explored, their major disadvantages being that they are energy intensive, have high capital costs or the slower reaction kinetics plus the possibility of contaminating the water with dissolved organics. Photocatalysis has emerged as a sustainable and clean approach for nitrate abatement, as it utilizes the inexhaustible solar energy and the selectivity of the reaction can be tuned to produce eco-friendly degradation products.

Many photocatalyst compositions have been proposed for nitrate transformation including Ag/TiO$_2$ on a chromium based MOF (AgMIL-101(Cr)),[13] Pd/GdCrO$_3$[14] PdSn/NiO/NaTaO$_3$:La,[15] ZnCrS$_4$,[16]

CuInS$_2$,[17] LiNbO$_3$[18] in addition to several different M/TiO$_2$ systems (M = Cu, Fe, Pt, Pd, Au, Ag, Sn). Promising nitrate conversion rates and selectivity to gaseous N$_2$ have been reported over these compositions, although a high NH$_4^+$ fraction has been observed in some instances[15, 19-21], and some of the proposed compositions require complex synthesis protocols. TiO$_2$ has been extensively studied for the remediation of environmental pollutants since its photocatalytic properties were demonstrated[22] mainly because it is environmentally benign, inexpensive, widespread availability and photo-stable. However, TiO$_2$ suffers from high recombination rates of the photo-generated holes and electrons, thus inhibiting its activity. Decorating titania with plasmonic nanoparticles is a versatile method which promotes the formation of a Schottky barrier between the semi-conductor and the metal nanoparticle. This can have the effect of extracting photo-generated electrons and thus limiting recombination of the charge carriers.[23] In addition to extending the electron/hole lifetime, the coinage metals such as Ag[24] and Au[25, 26] have also been shown to have a strong localized surface plasmon resonance (LSPR) and are capable of absorbing light and generating hot electrons which can be used for reduction reactions. To date, silver-decorated TiO$_2$ (Ag/TiO$_2$) has stood out as the most promising photocatalyst for nitrate degradation in aqueous solutions, displaying high reaction rates.[27, 28] It is therefore surprising that this catalyst has not been investigated in great detail.

In this study, we have used low-conversion conditions to probe the impact of incorporating Au and Ag co-catalysts on titania for the photocatalytic degradation of nitrate in waste waters. We demonstrate that the photocatalytic reduction of nitrate over Au/TiO$_2$ and Ag/TiO$_2$ catalysts can be tuned to selectively produce environmentally friendly N$_2$, and avoid the formation of harmful nitrite and ammonium intermediates. This was achieved by optimizing the catalyst preparation protocol, as well as the photocatalysis reaction conditions.

2 Experimental methods

2.1 Catalyst preparation

2.1.1 Incipient wetness impregnation

The Au/TiO$_2$ and Ag/TiO$_2$ catalysts with metal loadings in the range 0 – 1 wt.% were prepared by the incipient wetness impregnation method as previously reported.[29] Typically, Degussa P25 TiO$_2$ (51 m^2/g) was added to a 10 mL beaker and a solution of HAuCl$_4$.3H$_2$O or AgNO$_3$ added dropwise under stirring. The resulting paste was dried in an oven (110 °C, 16 hours) followed by calcination (400 °C, 3 h, 20 °C/min). The samples were subsequently sieved using a 53 micron sieve before catalytic tests.

2.1.2 Sol immobilization

To an aqueous solution of the metal precursor, citric acid was added to act as a stabilizer. After 10 min of stirring, excess NaBH$_4$ (Aldrich, 96%) (NaBH$_4$/M = 5) was added and the solution changed to a dark brown colour. The solution was stirred for a further 30 min before the required amount of TiO$_2$ added to make a 1 g batch of catalyst and the solution acidified to pH 2 with H$_2$SO$_4$. The reaction was allowed to proceed for 1 h, after which the catalyst was filtered under vacuum, washed and dried in an oven (110 °C, 16 h) and then calcined (400 °C, 3 h, 20 °C/min). Finally, the catalyst sieved with a 53 micron sieve.

2.2 Photocatalytic measurements

The photocatalytic reduction experiments were carried out at an initial nitrate concentration of 100 ppm (0.0016 M NaNO$_3$, Sigma-Aldrich). Formic acid was added as a hole scavenger with the required concentration explored as part of the investigation. The catalyst concentration was optimized to be 0.24 g/L and all experiments carried out under stirring. Prior to commencing degradation, the reaction mixture was kept in the dark for 30 minutes to attain an adsorption-desorption equilibrium of nitrate on the catalyst surface. A 300 W Xe arc lamp (irradiance: 1000 W/m^2) was used to mimic the average solar irradiance at sea level on the earth's surface. The nitrate degradation reaction was studied at low conversions to ensure limited mass transfer effects and also to improve selectivity to N$_2$. This was achieved by using a 500 mL open-top jacketed glass reactor for all our experiments, which is much larger than most reported systems. The open-top reactor configuration ensured direct introduction of the incident radiation to the reaction medium, eliminating possible shielding effects. Temperature control of the reaction was achieved by a thermo-

regulated water bath through the inlet port in the outer jacket of the vessel which then returns from the outlet port to the water bath in a cycle.

Two blank experiments were carried out to ensure that nitrate reduction was indeed photo-catalyzed. First, nitrate degradation was attempted under UV illumination for 3 h in the absence of a catalyst. Also, the transformation was tried in the dark in the presence of a catalyst. Both blank experiments were performed using the optimized formic acid concentration (see below). No appreciable nitrate conversion was observed in either case.

To determine the concentrations of different species as the reaction progressed, sample aliquots (2 mL) were withdrawn at specific time intervals during the photocatalytic degradation experiments and analysed for residual nitrate, nitrite and formate using ion chromatography on a Dionex ICS-1100 system equipped with a Dionex Ion Pac AS22 Fast column maintained at 30 °C. The eluent solution (4.5 mM Na_2CO_3/ 1.4 mM $NaHCO_3$) was pulsed at a flow-rate of 0.3 mL/min and changes in nitrate concentration were monitored using a conductivity detector. The injection volume was maintained at 10 μL. Nitrate conversion was calculated according to equation (1), where $[NO_3^-]_0$ and $[NO_3^-]_t$ are the nitrate concentrations at time = 0 and t, respectively. The error in the nitrate conversion measurements was estimated to be ~ 1.25% from repeated measurements of identical experiments.

$$\text{Nitrate conversion (\%)} = \left(\frac{[NO_3^-]_0 - [NO_3^-]_t}{[NO_3^-]_0}\right) x \ 100 \ \% \tag{1}$$

Ammonium ion formation during the reaction was monitored by using an ion selective electrode (Thermo Fisher Scientific) calibrated using 100, 50 and 25 ppm NH_4^+ standards prepared by dilution of a 1000 ppm ammonium chloride solution. Selectivities towards intermediate products such as dinitrogen, ammonium and nitrite ions were calculated using equations 2 − 4, respectively. $[NH_4^+]_t$ and $[NO_2^-]_t$ are the ammonium and nitrite ion concentrations in ppm.

$$\text{Dinitrogen selectivity } (S_{N_2}, \%) = 100 - (S_{NH_4^+} + S_{NO_2^-}) \tag{2}$$

$$\text{Ammonium selectivity } (S_{NH_4^+}, \%) = \left(\frac{[NH_4^+]_t}{[NO_3^-]_0 - [NO_3^-]_t}\right) x \ 100\% \tag{3}$$

$$\text{Nitrite selectivity } (S_{NO_2^-}, \%) = \left(\frac{[NO_2^-]_t}{[NO_3^-]_0 - [NO_3^-]_t}\right) x \ 100\% \tag{4}$$

3 Results and discussion

3.1 Optimization of catalyst preparation methodology

Since the preparation method can have a significant effect on a catalyst's behaviour, we started our investigation by optimising this aspect. The effect of sieving, drying, calcination and the sequence in which these steps were performed on the catalyst performance was explored. Fig. 1a shows how the rate of nitrate conversion can be affected by the sieving of a 1% Au/TiO_2 catalyst through a 53 μm mesh sieve. Nitrate transformation was improved by over 10 % relative to the un-sieved samples which can be attributed to the smaller overall agglomerate (grain) size of the sieved samples shown by dynamic light scattering (DLS). See below for a discussion of the DLS results. Fig. 1b compares the combined effects of the drying, sieving and calcination sequence on the Au/TiO_2 catalyst. Whilst the dry-calcine-sieve sample displayed slightly superior nitrate conversion compared to other sequences and was subsequently adopted for all samples, the overall effect of the sequence of these heat-treatment steps on the catalyst activity was minimal.
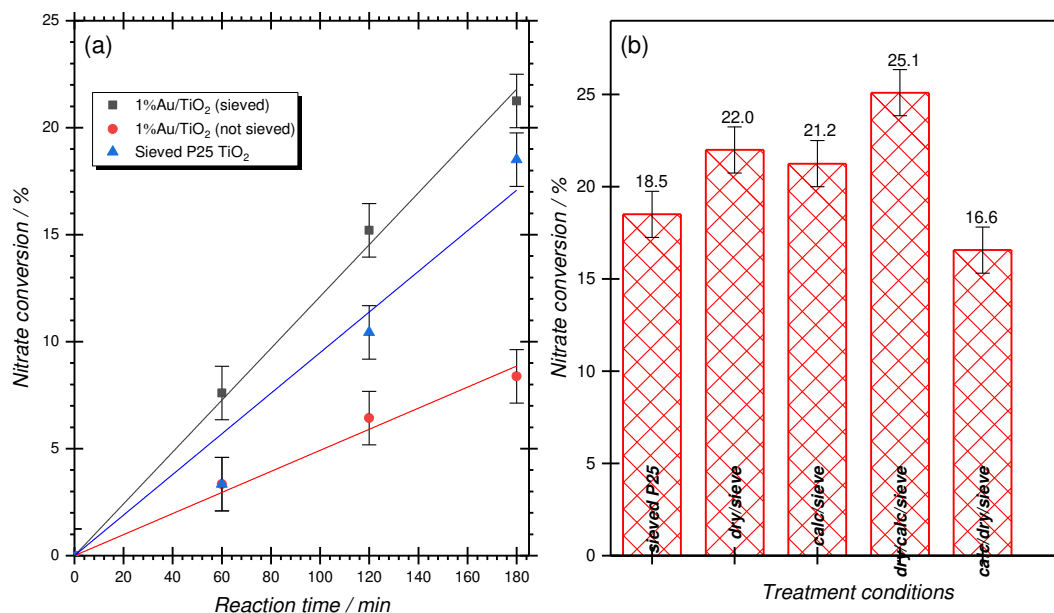
Figure 1: (a) Effect of the sieving step on nitrate conversion, and (b) influence of drying, sieving and calcination combinations on nitrate conversions analysed using the 1%Au/TiO$_2$ catalyst.

3.2 Effect of the preparation method and analysis conditions

Fig. 2a compares the activity of three 1%Au/TiO$_2$ catalysts with that of the unmodified P25 support. The calcined catalysts were characterized by BET, XRD and SEM-EDX techniques. Minimal surface area changes were seen on the catalysts *vis-à-vis* the P25 TiO$_2$ support (51.1 m^2/g), with the largest decrease measured on the Au/TiO$_2$ sample (48.4 m^2/g). These surface area values are comparable and within instrumental error. The co-catalyst crystallites were generally well-dispersed on the TiO$_2$ support, hence signals due to Au, Ag or Pd could not be detected by X-ray diffraction (XRD) as shown in Fig. S1. The dispersion of Au particles on TiO$_2$ was confirmed by SEM-EDX elemental mapping (Fig. S2).

The optimised incipient wetness impregnation catalyst displays superior activity with ~ 25 % conversion after 180 minutes (Fig. 2a). The sol based catalysts were less productive with the citrate-stabilization reducing activity even further. This could be because of the much smaller gold particles achieved using this approach[30] blocking more TiO$_2$ surface sites and minimizing the generation of electron-hole charge carriers upon photo-excitation, which are crucial for the photocatalytic process. Alternatively, encapsulation of the gold nanoparticles by residual citrate may prevent them from establishing a Schottky barrier with the TiO$_2$ substrate. For these studies, minimal pH changes were measured before and after the 3 h reaction when the different samples were tested. For instance, when undecorated P25 TiO$_2$ was tested for nitrate degradation the pH increased marginally from an initial 3.08 to 3.63 after the experiment. This observation was attributed to both the low conversion conditions used and the low selectivity to the ammonium by-product. It is to be noted that the same optimized concentration of the formic acid hole scavenger was used for catalyst evaluation tests, see below for the optimization studies.

Fig. 2b illustrates the effect of stirring the reaction media. This was tested by performing nitrate transformation under UV illumination, then at 120 minutes turning OFF both illumination and stirring. After 60 minutes under these conditions the illumination was switched back ON but the stirrer remained switched OFF (to allow time for the larger catalyst agglomerates to settle at the bottom of the reactor). Under normal operation (UV illumination, stirrer ON), a steady increase of up to 16 % nitrate conversion was observed for the first 120 min. From 120 – 180 min no appreciable change in nitrate conversion was observed because the Xe arc lamp and stirrer were both switched OFF. This further confirmed that this transformation is photo-catalyzed as no further reaction was observed when the incident radiation was switched OFF. Upon switching the lamp ON again (while the stirrer remained OFF), nitrate transformation was again observed to increase in the time interval of 180 – 300 min. Notably, in the last part of the experiment the stirring was switched OFF to allow the larger catalyst agglomerates to settle at the bottom of the reactor and not significantly influence the overall

conversion occurring within the reactor. Fig. 2b shows that the nitrate conversion with the stirrer OFF (180 – 300 min) was almost linear with the first part of the experiment when the stirrer was still ON. From these experiments we concluded that nitrate conversion is facilitated by the small catalyst grains, and to a lesser extent by the bigger grains. This observation is in good agreement with our experiments on the effect of catalyst sieving discussed earlier.

We performed dynamic light scattering (DLS) experiments in order to quantify the effect of stirring on the average grain size of the catalyst in solution. These experiments involved shaking a water-catalyst mixture to make a suspension. Then the suspension was allowed to settle in a cuvette placed inside the DLS instrument, and scans recorded at regular time intervals to determine the average aggregate size. Table S1 lists the average aggregate diameter recorded after agitation and waiting for 0 and 120 minutes without stirring. Immediately after agitation (i.e. 0 min waiting time), the average aggregate diameters were 6008 and 1021 nm for P25 TiO_2 and 0.3%Au/TiO_2, respectively. A significant decrease in the average aggregate size was observed after a 120 minutes waiting period because the heavier catalyst grains settled at the bottom of the cuvette while the smaller ones remained in solution. These results show that it is the smaller catalyst aggregates (with an average diameter of <1000 nm) doing most of the catalytic work. We can also see from the table that there is a considerable difference in average aggregate size between undecorated P25 TiO_2 and the metal-modified catalyst.
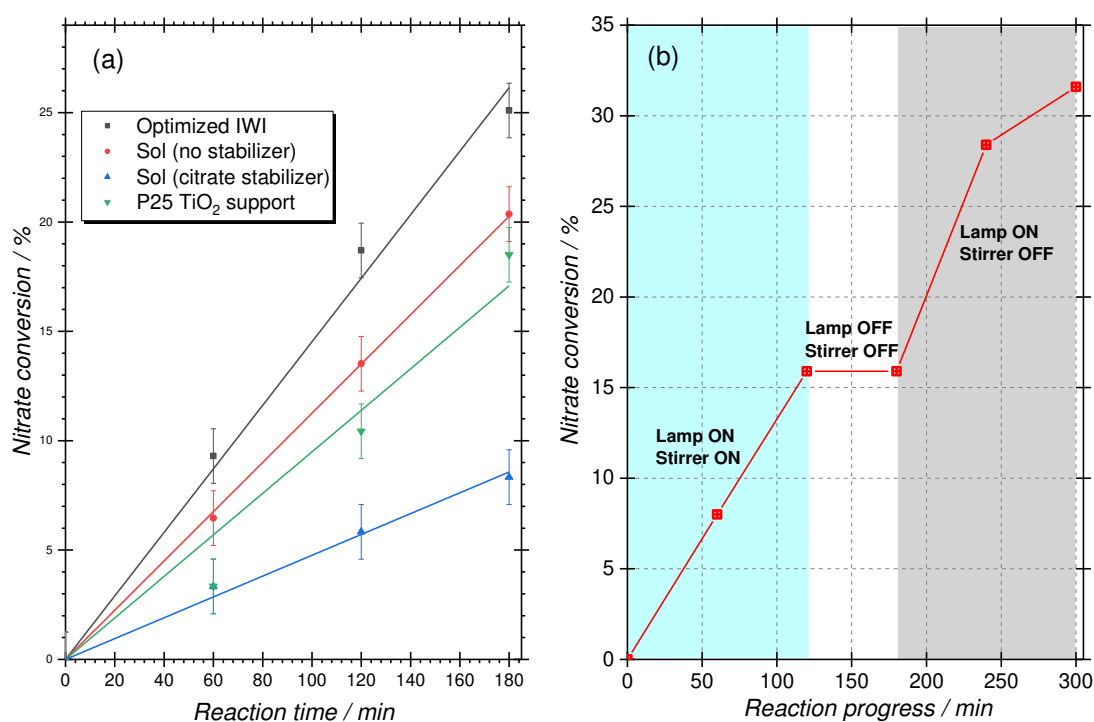

Figure 2: Dependence of nitrate conversion on (a) the catalyst preparation method and (b) stirring and switching the Xe arc lamp ON/OFF during the experiments.

3.3   Nitrate transformation on 0.3 wt.% M catalysts

We have also explored the use of Pd as a co-catalyst for comparison with the Ag and Au under similar metal loadings. A 0.3%Pd/TiO_2 catalyst was prepared using the optimized impregnation protocol and it yielded an inactive PdO/TiO_2 material.[31] To improve the rate of nitrate degradation, the prepared material was either reduced under the flow of pure H_2 (400 °C) then calcined (sample denoted as 0.3%Pd/TiO_2-red-calc), or calcined and then reduced at the same reaction temperature (sample denoted as 0.3%Pd/TiO_2-red). Fig. 3a shows that the heat treated Pd samples displayed improved nitrate conversion rates relative to the as-prepared material, but these activities were still much lower than those measured on the Ag- or Au-doped TiO_2 catalysts. In fact, the NO_3^- conversion observed on the 0.3%Pd/TiO_2-red-calc sample was only marginally better than undoped TiO_2. It was interesting to note that despite the large differences in nitrate transformation, formate conversions were quite similar for these samples and were in the range 56 – 65 % after 3 h of reaction (Fig. 3b).
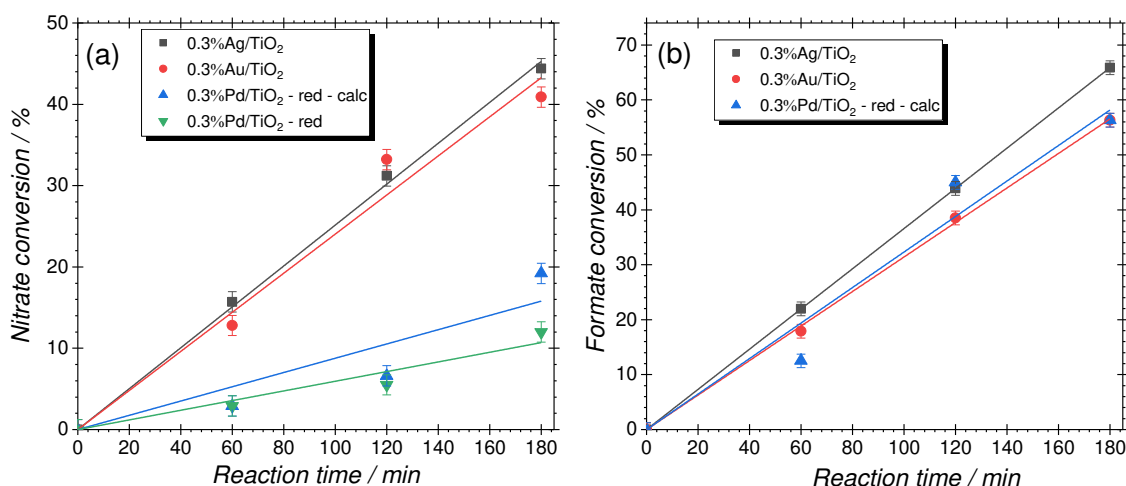
Figure 3: Comparison of activities of 0.3%M/TiO$_2$ for (a) photo-reduction of nitrates, and (b) photo-oxidation of formic acid.

3.4 The role of the hole scavenger

The choice of sacrificial agent to scavenge the valence band holes generated by the photoexcitation and balance the nitrate reduction has a significant impact on the efficiency of nitrate reduction; a rapid rate of the oxidation reaction reducing the likelihood of electron hole recombination. By comparing solvents such as ethanol, oxalic acid, sodium oxalate, acetic acid, formic acid and sodium formate, previous studies have shown that formic acid is a superior electron hole scavenger for nitrate photocatalytic transformation.[4, 28] In this study we have studied the effects associated with the concentration of the formate scavenger and its addition as the reaction progresses. Fig. 4a demonstrates the photocatalytic activity dependence of the scavenger concentration. 0.008 and 0.016 M formate solutions yielded similar nitrate conversions of ~33 %, most likely because the minimum concentration had been achieved. However, lower nitrate conversions were measured when 0.004 M formic acid was used. For all subsequent experiments the formic acid concentration was therefore maintained at 0.008 M. Fig. 4b shows the effect of formate addition (0.0092 M) after the reaction had been in progress for 240 min. After this formate addition, nitrate conversion doubled (Fig. 4b) illustrating that the depletion of the formate hole scavenger was responsible for the tapering of the activity observed at 240 min, likely *via* poor electron-hole charge segregation. In addition, this result also illustrated that the formate ion is an effective hole scavenger for this reaction.
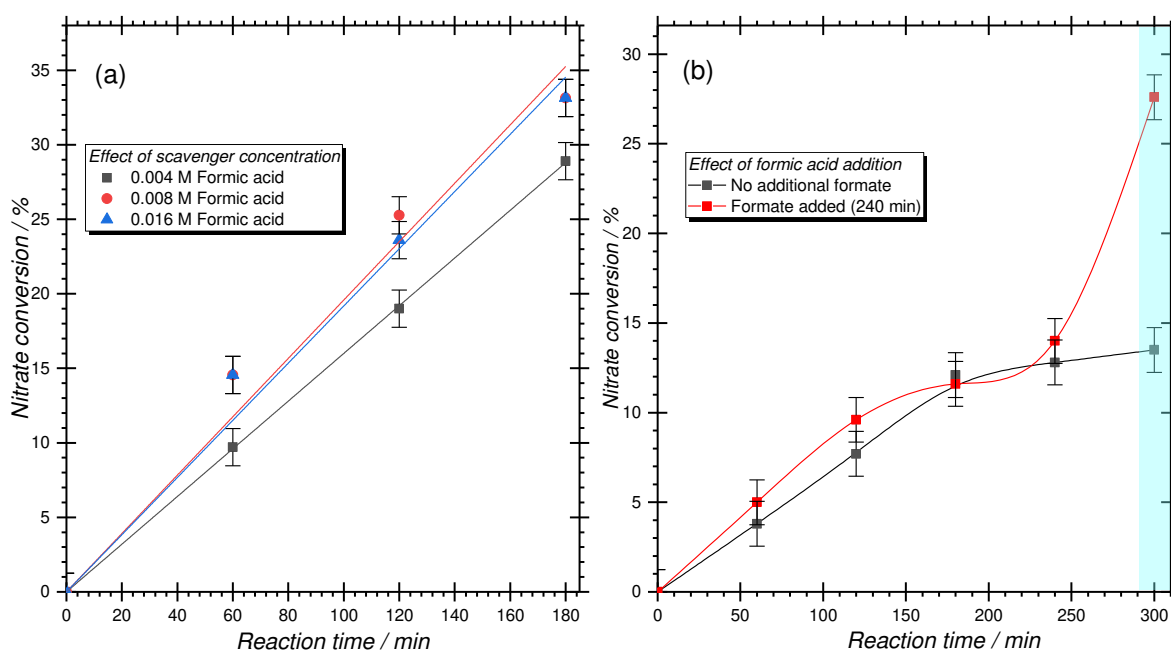

6

Figure 4: Percentage of nitrate converted vs time on different starting concentrations of formic acid (0.2%Au/TiO$_2$ catalyst). (b) Effect of formic acid addition as nitrate conversion tapers off (1%Au/TiO$_2$ catalyst).

3.5 Impact of metal loading

Fig. 5 and Table 1 summarizes the nitrate conversions as well as the selectivity to N$_2$ measured on TiO$_2$ supported gold and silver catalysts after a 3 h reaction time. We noted that nitrate degradation adopts the form of a volcano plot, going through a maxima as a function of the metal content and then declining at higher metal loadings. For Au catalysts, the maximum nitrate transformation activity was observed at a metal loading of 0.2 wt.% where 55 % of the starting contaminant was degraded. For comparison, much lower activity was measured on the Ag/TiO$_2$ catalyst at a similar loading of 0.2 wt.%, illustrating the differences between the two catalytic systems. The maximum activity on the Ag/TiO$_2$ samples was observed at a metal ratio of 0.4 wt.% where nitrate conversions of up to 57 % were recorded. Increasing the metal loading on both systems beyond the optimum loading drastically decreased the activity, with nitrate conversions as low as 15 and 26 % measured on the Ag and Au samples at a 0.6wt% loading, respectively.

Photocatalytic reduction of nitrates is known to yield a mixture of products that consist of NO$_2^-$, NH$_4^+$ and N$_2$. Our photo-reduction experiments were generally highly selective to dinitrogen gas formation over the studied catalysts as summarized in Table 1. Other possible side-products such as nitrosamines and N-based dimers were not detected in this study. When P25 TiO$_2$ was tested as the photocatalyst under these low conversion conditions, N$_2$ was produced exclusively. Nitrite and NH$_4^+$ ions were not detected when undecorated TiO$_2$ was used as the photo-catalyst, in agreement with other studies.[28] For the Ag/TiO$_2$ catalysts, nitrite formation was observed with up to 22 % detected at 0.1wt.% Ag loading. Increasing the Ag metal content enhanced N$_2$ selectivity as nitrite ions were not detected for catalysts with Ag loading > 0.3wt%. A different trend was observed for the Au/TiO$_2$ samples. Unlike the Ag samples, the catalysts with low Au loadings exclusively produced dinitrogen gas. Meanwhile small quantities of ammonia were detected on the highly active Au samples with 0.2 − 0.3 wt.% loading. Previous studies have shown that high nitrate conversions can lead to an increased formation of undesirable NH$_4^+$ intermediate on Au catalysts.[20] Nitrite formation was not observed on the Au samples. This is attributed to the fast nitrite to dinitrogen transformation that occurs on Au-decorated TiO$_2$ photo-catalysts.
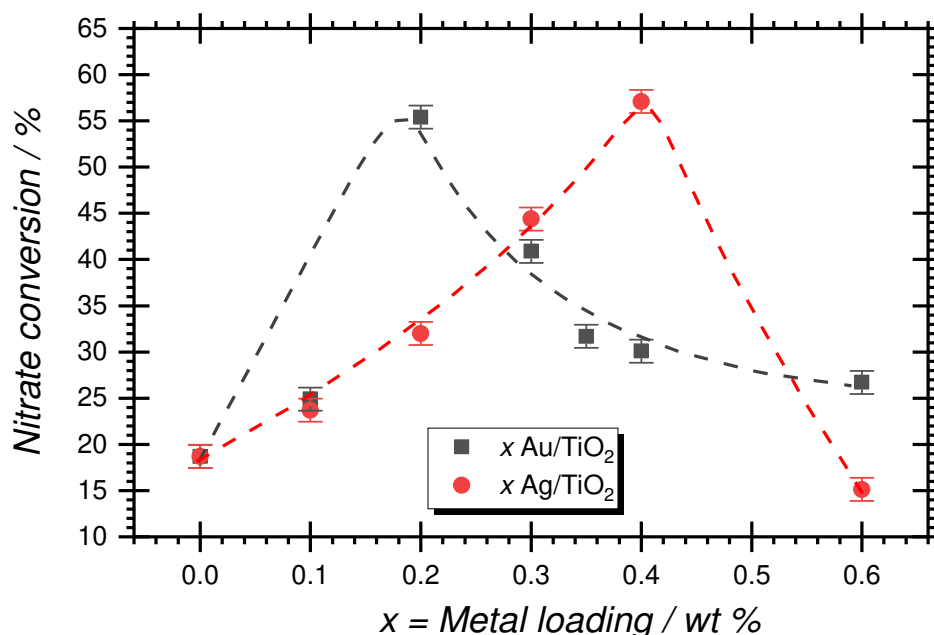

Figure 5: Effect of Au and Ag loading (wt. %) on nitrate conversions measured after a 3 h reaction time.

Metal loading (wt.%)	Catalyst: Au/TiO$_2$, 3 h[a]			Catalyst: Ag/TiO$_2$, 3 h[b]		
	NO$_3^-$ conversion (%)	N$_2$ selectivity (%)	NH$_4^+$ selectivity (%)	NO$_3^-$ conversion (%)	N$_2$ selectivity (%)	NO$_2^-$ selectivity (%)
0.1	24.9	100	n.d.	23.7	77.7	22.3
0.2	55.4	99.3	0.7	32.0	-	-
0.3	40.9	97.1	2.9	44.4	94.5	5.5
0.4	30.1	100	n.d.	57.1	100	n.d.
0.6	26.7	100	n.d.	15.1	100	n.d.

[a]Nitrite ion was not detected (n.d.) over Au/TiO$_2$ catalysts; [b]Ammonium ion was not detected (n.d.) over Ag/TiO$_2$ catalysts

Table 1: Nitrate conversion and selectivity to N$_2$ on Au/TiO$_2$ and Ag/TiO$_2$ catalysts after 3 h reaction.

Previous studies have shown that the metal content and the catalyst preparation method can influence the photocatalytic degradation of pollutants. For catalysts prepared by photo-decomposition (1 g/L), Zhang *et al.* found that 1%Ag/TiO$_2$ displayed the highest nitrate degradation rate while higher silver loadings such as 2%Ag/TiO$_2$ resulted in increased NO$_2^-$ selectivity.[28] Elsewhere photo-deposition of Ag onto TiO$_2$ (Hombikat) was noted to decrease dinitrogen selectivity when the metal content was increased.[4] More recently, nitrate transformation has been reported to improve with the Ag loading on a Zn-Ag bimetallic system, accompanied by decrease in NH$_4^+$ and NO$_2^-$ selectivity.[32] For Au-decorated catalysts, photo-transformation of nitrate or nitrite has been shown to result in over-reduction thus yielded a significant fraction of the ammonium ion by-product.[20, 33] Meanwhile, studies of Pd by Hou *et al.* recently analysed Pd/GdCrO$_3$ catalysts and found that the 1wt.% loading was optimum for nitrate degradation, displaying a higher activity than 0.5 and 2wt% loadings.[14]

To improve catalytic conversion, the use of electron hole scavengers has been proposed as an effective strategy for minimizing the recombination of photo-generated charge carriers. Whilst a few studies have reported that hole scavengers such as oxalic acid or formic acid can inhibit nitrate photo-reduction coupled with the undesirable selectivity towards ammonia,[34, 35] it has been demonstrated that by the quantity of hole scavenger can be optimized so as to prolong the availability of the photo-generated electrons thus enhance the reduction of nitrates.[36] Anderson *et al.* compared hole scavengers such as formic acid, acetic acid, sodium formate and sodium acetate and found that the use of formic acid yielded the highest rate for nitrate transformation, although a decrease in dinitrogen selectivity was noted at high conversions due to over-reduction to ammonia.[4] In our studies, we have evaluated the activity of our catalysts under low conversion conditions to minimize the formation of undesirable side-products, and we used an optimized concentration of the formic acid hole scavenger. Under these conditions, selectivity towards ammonia was minimal (Table 1) as it was only detected on the highly active Au/TiO$_2$ samples with metal loadings in the range $0.2 - 0.3$ wt%. The nitrite by-product was only detected over Ag/TiO$_2$ catalysts. Furthermore, we found that addition of formic acid when the reaction had tapered off (240 min) resulted in improved nitrate degradation which illustrates the promotional effect of the hole scavenger, see Fig. 4b.

3.6   Photo-reduction of nitrates on bimetallic catalysts

Synergistic effects of Au and Ag were explored by studying different metal ratios for the photodegradation of nitrates and are displayed in Fig. 6. Synthesis of the bimetallic samples was performed using the methodology developed in our group to favour alloy formation as previously reported.[37, 38] For the batch of samples under study, the 0.3%Au-0.3%Ag/TiO$_2$ bimetallic sample displayed the highest nitrate conversion rate (48 %), followed by the 0.3%Ag/TiO$_2$ and 0.3%Au/TiO$_2$ monometallic samples with 44 and 41 % conversion respectively (Fig. 6). Low photocatalytic activity was observed on the 0.15%Au-0.15%Ag/TiO$_2$ and 0.3%Au-0.15%Ag/TiO$_2$ bimetallic samples, the recorded nitrate conversions were similar to pure P25 TiO$_2$. These findings demonstrate that the bimetallic samples did not possess additive properties of the monometallic samples, instead they were observed to have different catalytic characteristics. For instance, the high nitrate degradation of 48 % measured on the 0.3%Au-0.3%Ag/TiO$_2$ bimetallic sample was much lower than the rate that could be expected from the additive effects of its monometallic constituents (0.3%Au/TiO$_2$ and 0.3%Ag/TiO$_2$).

It seems that alloy formation on the bimetallic samples did not have a positive effect on nitrate conversion. This observation was further illustrated by the 0.15%Au-0.15%Ag/TiO$_2$ sample which had the lowest activity (20 % conversion), which is much lower than the monometallic catalysts with a metal content of 0.3 wt%.
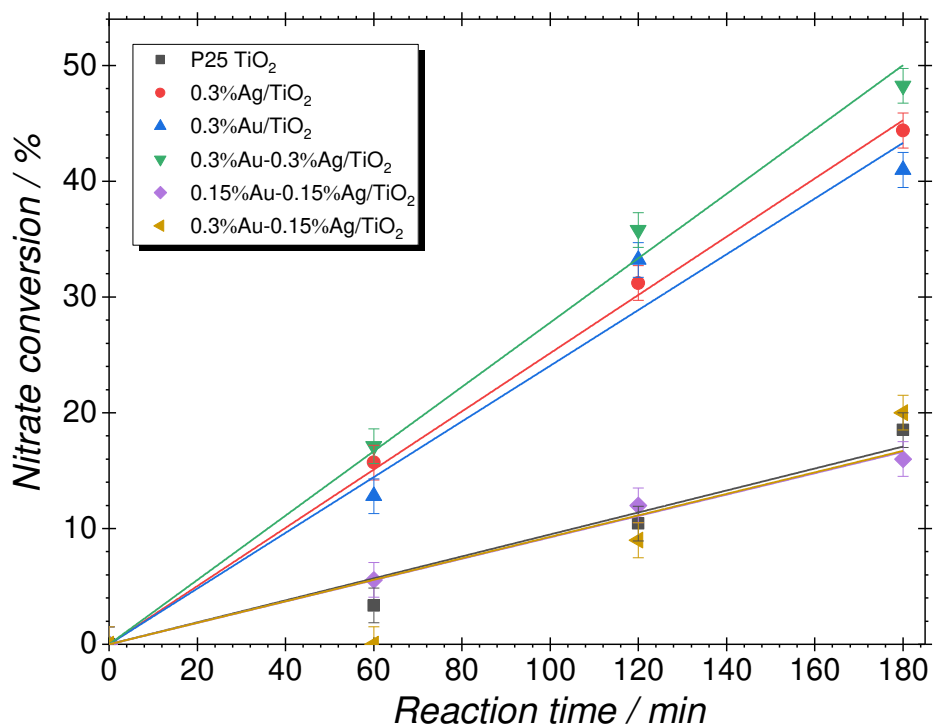

Figure 3: Photocatalytic nitrate conversion rates measured on mono- and bimetallic samples.

Photo-reduction of nitrates has been shown to occur by pseudo first-order reaction kinetics as summarized by equation 5, where C$_o$ and C$_i$ are the nitrate concentrations at $t = 0$ and $t = i$, respectively ($i = 0, 60, 120, 180$).

$$ln(\frac{C_o}{C_i}) = k\text{t} \tag{5}$$

Table 2 and Fig. S3 (supplementary information) depicts the pseudo first-order rate constants (k) of the mono- and bi-metallic decorated samples relative to TiO$_2$. The k values further quantify the slight improvement in activity introduced by doubling the metal content on the 0.3%Au-0.3%Ag/TiO$_2$ sample, relative to the best performing Au and Ag monometallic catalysts. On Table 2, the k values illustrate that alloying Au and Ag generally did not enhance the degradation of nitrates as low rate constants were measured.

Photocatalyst	First-order rate constant / s^{-1}
TiO$_2$	1.6 x 10^{-3}
0.3 % Ag/TiO$_2$	4.2 x 10^{-3}
0.3 % Au/TiO$_2$	4.0 x 10^{-3}
0.3 % Au - 0.3 % Ag/TiO$_2$	4.6 x 10^{-3}
0.15 % Au - 0.15 % Ag/TiO$_2$	1.5 x 10^{-3}
0.3 % Au - 0.15 % Ag/TiO$_2$	1.6 x 10^{-3}

Table 2: Pseudo first-order rate constants calculated for the mono- and bimetallic catalyst systems.

3.7   Recyclability of the catalysts

Fig. 7 shows the nitrate and formate conversions for a 0.3%Au/TiO$_2$ catalyst that was re-analysed to test the recyclability of the samples. Recycling the catalysts involved collecting the spent samples after a 3h reaction time, filtering and washing with deionized water before being oven dried (110 °C, 16 h). The catalyst was then re-sieved and tested under identical reaction conditions to the experiments with the fresh samples. The data in Fig. 7 indicates that the catalyst activity remains largely unchanged with regards to both formic acid oxidation and nitrate reduction upon re-use, and correlates well with previous literature reports.[39] The N$_2$ selectivity was also found to be unchanged upon re-use.
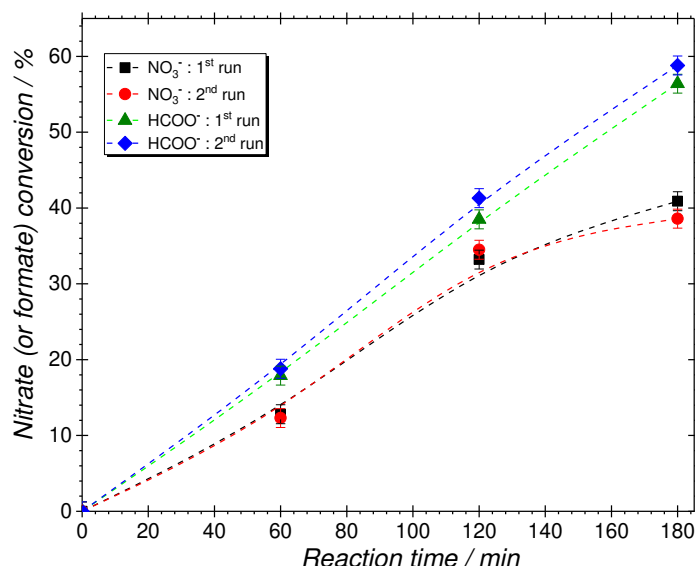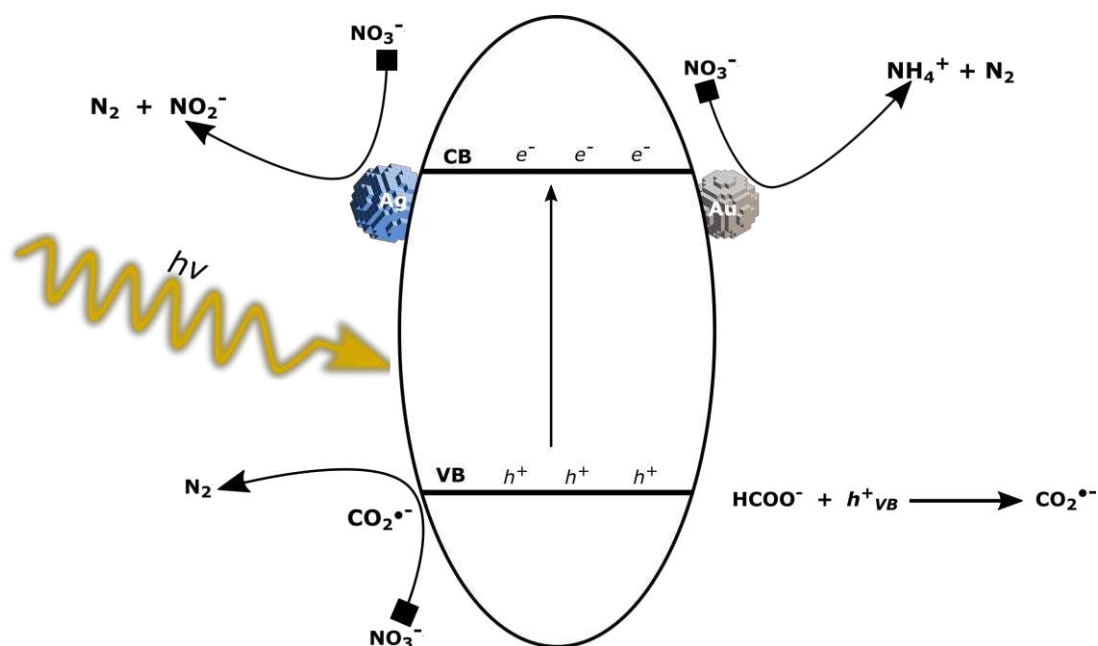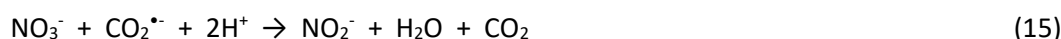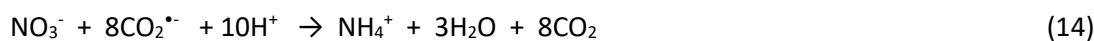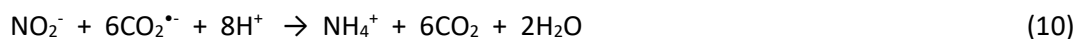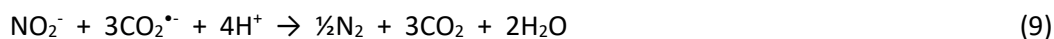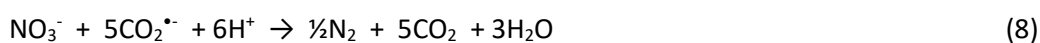

Figure 4: Nitrate and formate conversions measured on recyclability tests of the 0.3%Au/TiO$_2$ catalyst.

3.8   Nitrate photo-reduction reaction mechanism

The partial dissociation of formic acid in aqueous solutions to HCOO$^-$ (pKa = 3.75), is known to lead to the CO$_2$$^{\bullet-}$ species through scavenging of the photo-generated holes, Eq. 7. The strong reductive ability of CO$_2$$^{\bullet-}$ (E^o(CO$_2$/ CO$_2$$^{\bullet-}$) = -1.8 V) is capable of converting both nitrate and nitrite, to N$_2$ (E°(NO$_3^-$/N$_2$) = 1.25 V and E°(NO$_2^-$/N$_2$) = 1.45 V) but also of converting the nitrite to ammonium (E°(NO$_2^-$/NH$_4^+$) = 0.897 V) as illustrated in Eq. 8 – 10.[21, 40] Direct reduction of the nitrate and nitrite to N$_2$, NH$_4^+$ and NO$_2^-$ could also proceed *via* the photo-generated electrons Eq. 11 – 13.[41] There is a significant difference between the Au- and Ag-doped catalysts. Over the former, N$_2$ is the main product with minute NH$_4^+$ quantities at high nitrate conversion rates whereas over the Ag/TiO$_2$ catalyst with Ag < 0.4 wt% nitrite is the main by-product to N$_2$. The different product distributions suggest different mechanisms over the two metals which needs to be explored in future studies.

Scheme 1: Proposed nitrate photo-reduction mechanism on Au/TiO_2 and Ag/TiO_2 catalysts when formic acid is used as a hole scavenger.

$$TiO_2 + h\nu \rightarrow e^- + h^+ \tag{6}$$

$$HCOO^- + h^+ \rightarrow CO_2^{\bullet-} + H^+ \tag{7}$$

$$NO_3^- + 5CO_2^{\bullet-} + 6H^+ \rightarrow \tfrac{1}{2}N_2 + 5CO_2 + 3H_2O \tag{8}$$

$$NO_2^- + 3CO_2^{\bullet-} + 4H^+ \rightarrow \tfrac{1}{2}N_2 + 3CO_2 + 2H_2O \tag{9}$$

$$NO_2^- + 6CO_2^{\bullet-} + 8H^+ \rightarrow NH_4^+ + 6CO_2 + 2H_2O \tag{10}$$

$$NO_3^- + 6H^+ + 5e^- \rightarrow \tfrac{1}{2}N_2 + 3H_2O \tag{11}$$

$$NO_3^- + 10H^+ + 8e^- \rightarrow NH_4^+ + 3H_2O \tag{12}$$

$$NO_3^- + 2H^+ + 2e^- \rightarrow NO_2^- + H_2O \tag{13}$$

$$NO_3^- + 8CO_2^{\bullet-} + 10H^+ \rightarrow NH_4^+ + 3H_2O + 8CO_2 \tag{14}$$

$$NO_3^- + CO_2^{\bullet-} + 2H^+ \rightarrow NO_2^- + H_2O + CO_2 \tag{15}$$

4 Conclusion

We have investigated the impact of Au and Ag co-catalysts on nitrate photocatalytic reduction under low conversion conditions. We have optimised the incipient wetness impregnation protocol for catalyst preparation and demonstrate that the dry-calcine-sieve sequence of steps improved the rate of nitrate transformation, with the sieving step shown to be particularly important. More significantly, we have shown that activity and selectivity of Au/TiO_2 and Ag/TiO_2 catalysts during photocatalytic nitrate transformation is dependent on the metal content and thus can be tuned. For both catalysts, high catalyst activity was measured on samples with low metal loadings, but higher loadings generally displayed poor nitrate conversion rates. Differences between the two catalysts are noted in their product selectivity towards the desired harmless N_2 product. At low loadings silver-doped titania resulted in low selectivity to nitrogen, producing up to 22 % nitrite ion while exclusive production of N_2 was only achieved for Ag loading > 0.3 wt%. Meanwhile Au-decorated titania photocatalysts were selective towards N_2 at low and high metal loadings, with small quantities of the ammonium ion detected for the highly active samples with intermediate metal content due to the over-reduction of

nitrate. The study of these two co-catalysts allowed us to conclude that reduction by the photo-generated $CO_2^{\bullet-}$ species results in the exclusive formation of dinitrogen gas. We did not observe any synergistic effects between Au and Ag co-catalysts as the bimetallic samples generally displayed low nitrate degradation rates.

Conflict of interest

There are no conflicts to declare.

Acknowledgements

5   References

1.   M. H. Ward, T. M. deKok, P. Levallois, J. Brender, G. Gulis, B. T. Nolan, J. VanDerslice and E. International Society for Environmental, *Environ. Health Perspect.*, 2005, **113**, 1607-1614.

2.   J. N. Galloway, A. R. Townsend, J. W. Erisman, M. Bekunda, Z. Cai, J. R. Freney, L. A. Martinelli, S. P. Seitzinger and M. A. Sutton, *Science*, 2008, **320**, 889-892.

3.   C. Holton, *Environ. Health Perspect.*, 1996, **104**, 36-38.

4.   J. Sá, C. A. Agüera, S. Gross and J. A. Anderson, *Appl. Catal. B*, 2009, **85**, 192-200.

5.   J. A. Camargo and Á. Alonso, *Environ. Int.*, 2006, **32**, 831-849.

6.   L. Xie, Y. Zhang, Y. Qu, L. Chai, X. Li and H. Wang, *Chemosphere*, 2019, **235**, 227-238.

7.   U.S.E.P.A., National Primary Drinking Water Regulations, https://www.epa.gov/ground-water-and-drinking-water/national-primary-drinking-water-regulations, (accessed 12-09-2019, 2019).

8.   E. Li, R. Wang, X. Jin, S. Lu, Z. Qiu and X. Zhang, *Environ. Technol.*, 2018, **39**, 2203-2214.

9.   I. Berkani, M. Belkacem, M. Trari, F. Lapicque and K. Bensadok, *J. Environ. Chem. Eng.*, 2019, **7**, 102951.

10. F. Djouadi Belkada, O. Kitous, N. Drouiche, S. Aoudj, O. Bouchelaghem, N. Abdi, H. Grib and N. Mameri, *Sep. Purif. Technol.*, 2018, **204**, 108-115.

11. P. S. Romer, P. J. Wooldridge, J. D. Crounse, M. J. Kim, P. O. Wennberg, J. E. Dibb, E. Scheuer, D. R. Blake, S. Meinardi, A. L. Brosius, A. B. Thames, D. O. Miller, W. H. Brune, S. R. Hall, T. B. Ryerson and R. C. Cohen, *Environ. Sci. Technol.*, 2018, **52**, 13738-13746.

12. O. Svoboda, L. Kubelová and P. Slavíček, *J. Phys. Chem. A*, 2013, **117**, 12868-12877.

13. X. Yang, X. Qi, G. Ma, Z. Li, Q. Liu, S. Khan, Y. Zhao, L. Zhang, Z. Geng and Y. Guo, *Appl. Surf. Sci.*, 2019, **479**, 1048-1056.

14. Z. Hou, F. Chen, J. Wang, C. P. François-Xavier and T. Wintgens, *Appl. Catal. B*, 2018, **232**, 124-134.

15. N. Tong, Y. Wang, Y. Liu, M. Li, Z. Zhang, H. Huang, T. Sun, J. Yang, F. Li and X. Wang, *J. Catal.*, 2018, **361**, 303-312.

16. M. Yue, R. Wang, N. Cheng, R. Cong, W. Gao and T. Yang, *Sci. Rep.*, 2016, **6**, 30992.

17. M. Yue, R. Wang, B. Ma, R. Cong, W. Gao and T. Yang, *Catal. Sci. Technol.*, 2016, **6**, 8300-8308.

18. G. Liu, S. You, M. Ma, H. Huang and N. Ren, *Environ. Sci. Technol.*, 2016, **50**, 11218-11225.

19. H. Kominami, A. Furusho, S.-y. Murakami, H. Inoue, Y. Kera and B. Ohtani, *Catal. Lett.*, 2001, **76**, 31-34.

20. J. A. Anderson, *Catal. Today*, 2012, **181**, 171-176.

21. H. Adamu, A. J. McCue, R. S. F. Taylor, H. G. Manyar and J. A. Anderson, *Appl. Catal. B*, 2017, **217**, 181-191.

22. A. Fujishima and K. Honda, *Nature*, 1972, **238**, 37-38.

23. C. Han, Q. Quan, H. M. Chen, Y. Sun and Y.-J. Xu, *Small*, 2017, **13**, 1602947.

24. F. Shi, J. He, B. Zhang, J. Peng, Y. Ma, W. Chen, F. Li, Y. Qin, Y. Liu, W. Shang, P. Tao, C. Song, T. Deng, X. Qian, J. Ye and J. Wu, *Nano Lett.*, 2019, **19**, 1371-1378.

25. H. Lee, H. Lee and J. Y. Park, *Nano Lett.*, 2019, **19**, 891-896.

26. J. Zhou, J. Zhang, H. Yang, Z. Wang, J.-a. Shi, W. Zhou, N. Jiang, G. Xian, Q. Qi, Y. Weng, C. Shen, Z. Cheng and S. He, *Nanoscale*, 2019, **11**, 11782-11788.

27. K. N. Heck, S. Garcia-Segura, P. Westerhoff and M. S. Wong, *Acc. Chem. Res.*, 2019, **52**, 906-915.

28. F. Zhang, R. Jin, J. Chen, C. Shao, W. Gao, L. Li and N. Guan, *J. Catal.*, 2005, **232**, 424-431.

29. M. Sankar, Q. He, M. Morad, J. Pritchard, S. J. Freakley, J. K. Edwards, S. H. Taylor, D. J. Morgan, A. F. Carley, D. W. Knight, C. J. Kiely and G. J. Hutchings, *ACS Nano*, 2012, **6**, 6600-6613.

30. L. Abis, N. Dimitratos, M. Sankar, S. J. Freakley and G. J. Hutchings, *Catal. Lett.*, 2019, DOI: 10.1007/s10562-019-02952-y, DOI: 10.1007/s10562-10019-02952-y.

31. P. Granger, S. Troncéa, J. P. Dacquin, M. Trentesaux, O. Gardoll, N. Nuns and V. I. Parvulescu, *Appl. Catal. B*, 2019, **253**, 391-400.

32. X. Gong, Y. Liu, B. Wang, W. Yang, L. Fan and Y. Liu, *Sci. Total Environ.*, 2019, **683**, 89-97.

33. A. Pandikumar, S. Manonmani and R. Ramaraj, *Catal. Sci. Technol.*, 2012, **2**, 345-353.

34. E. Bahadori, M. Compagnoni, A. Tripodi, F. Freyria, M. Armandi, B. Bonelli, G. Ramis and I. Rossetti, *Mater. Today-Proc.*, 2018, **5**, 17404-17413.

35. Y. Li and F. Wasgestian, *J. Photoch. Photobio. A*, 1998, **112**, 255-259.

36. S. Challagulla, K. Tarafder, R. Ganesan and S. Roy, *J. Phys. Chem. C*, 2017, **121**, 27406-27416.

37. M. Sankar, N. Dimitratos, P. J. Miedziak, P. P. Wells, C. J. Kiely and G. J. Hutchings, *Chem. Soc. Rev.*, 2012, **41**, 8099-8139.

38. G. J. Hutchings and C. J. Kiely, *Acc. Chem. Res.*, 2013, **46**, 1759-1772.

39. J. Li, M. Li, X. Yang, S. Wang, Y. Zhang, F. Liu and X. Liu, *ACS Appl. Mater. Interfaces*, 2019, **11**, 33859-33867.

40. W. Gao, R. Jin, J. Chen, X. Guan, H. Zeng, F. Zhang and N. Guan, *Catal. Today*, 2004, **90**, 331-336.

41. H. Zhang, Z. Liu, Y. Li, C. Zhang, Y. Wang, W. Zhang, L. Wang, L. Niu, P. Wang and C. Wang, *Appl. Surf. Sci.*, 2020, **503**, 144092.